Bull Earthquake Eng (2017) 15:2645–2671
DOI 10.1007/s10518-017-0089-7

ORIGINAL RESEARCH PAPER

Physics-based seismic input for engineering applications: a case study in the Aterno river valley, Central Italy

Lorenza Evangelista[1] · Sergio del Gaudio[2] · Chiara Smerzini[3] · Anna d'Onofrio[4] · Gaetano Festa[2] · Iunio Iervolino[5] · Luigi Landolfi[6] · Roberto Paolucci[3] · Antonio Santo[4] · Francesco Silvestri[4]

Received: 6 August 2016 / Accepted: 13 January 2017 / Published online: 24 January 2017

Abstract In this paper, we present 3D physics-based numerical simulations, in the near-source region at the regional scale, of the 2009, April 6, L'Aquila earthquake (central Italy), based on improved models of the Aterno river basin geology and source kinematics. The simulations were carried out by an open-source code, SPEED, based on a discontinuous Galerkin spectral element method. The numerical mesh of the Aterno basin was built on a detailed subsurface geological model and on the evaluation of the dynamic

Luigi Landolfi: Formerly at University of Naples, Federico II, Naples, Italy.

✉ Lorenza Evangelista
lorenza.evangelista@cnr.it

Sergio del Gaudio
sergio.delgaudio@unina.it

Chiara Smerzini
chiara.smerzini@polimi.it

Anna d'Onofrio
donofrio@unina.it

Gaetano Festa
festa@na.infn.it

Iunio Iervolino
iunio.iervolino@unina.it

Luigi Landolfi
luigi.landolfi@unina.it

Roberto Paolucci
roberto.paolucci@polimi.it

Antonio Santo
santo@unina.it

Francesco Silvestri
francesco.silvestri@unina.it

[1] Institute for Coastal Marine Environment, National Research Council, Naples, Italy

properties of the soils. The source model was selected among the kinematic solutions available in the literature as the one that fits best the near-source observations. Broadband ground motions were then generated through a hybrid method, combining 3D low frequency waveforms with high-frequency stochastic synthetics. To provide an example of application as seismic input to earthquake engineering analyses in the time domain, results of this approach were used for 2D site response analyses at Castelnuovo, a village severely damaged by the earthquake, and in the neighborhood of which no seismic record was available. SPEED simulation satisfactorily reproduces the recorded accelerograms in the frequency range 0.1–0.7 Hz. The site response analysis at the local scale shows that the amplification of the hill is more significant at its natural frequency, due to topographic and stratigraphic factors, than at the peak of the seismic input simulated by SPEED, that is at about 3 s along the fault-normal component. The presented application supports the conclusion that 3D physics-based numerical simulations do have the potential to become an alternative for determination of input ground motion for earthquake engineering analyses, especially for those scenarios for which real records are not available.

Keywords Near-source ground motion · 3D physics-based numerical simulations · Abruzzo earthquake · Site response analysis

1 Introduction

Earthquake engineering analyses in the time domain require input motions the selection of which is typically based on either (1) artificial accelerograms or (2) records from real earthquakes (e.g., Bommer and Acevedo 2004; Douglas and Aochi 2008; NIST 2011). Spectrum-compatible signals of type (1) are obtained, for example, generating a power spectral density function from a code-specified response spectrum, and deriving signals compatible with that spectrum. However, this approach may lead to accelerograms not reflecting the real phasing of seismic waves and cycles of motion (Iervolino et al. 2010a). Presently this class of methods has become less relevant, owing to the increase in both quantity and quality of earthquake recordings. This approach is becoming more and more widespread in practice, because the availability of open-source, user-friendly, databases of strong-motion recordings, together with the rapid development of digital seismic networks worldwide, has increased the accessibility to good-quality recorded accelerograms, which are the most desirable candidates for the seismic assessment of structures, both for code-related purposes and probabilistic risk analysis (e.g., Iervolino et al. 2010b, 2011; Smerzini et al. 2014). However, real records may not always cover the whole range of magnitude and distance scenarios of interest for specific earthquake engineering applications. More

[2] Department of Physics, University of Naples Federico II, Naples, Italy

[3] Department of Civil and Environmental Engineering, Politecnico di Milano, Milan, Italy

[4] Department of Civil, Architectural and Environmental Engineering, University of Naples Federico II, Naples, Italy

[5] Department of Structures for Engineering and Architecture, University of Naples Federico II, Naples, Italy

[6] ASTALDI s.p.a., Rome, Italy

specifically, they are typically insufficient to represent large magnitude crustal events in near-source conditions, especially if coupled with complex geological and morphological irregularities, as in the case of deep basins (Koketsu and Miyake 2008) or hanging-wall effects (Donahue and Abrahamson 2014).

To effectively cope with such limitations, physics-based source-to-site numerical simulations are becoming a third alternative to produce reliable input motions for earthquake engineering applications, which is worth of investigating. This approach consists of the combined modeling of the earthquake faulting process, of the propagation path and of the local site topographic and geologic effects. Different classes of methods are available for this purpose, including (a) the Empirical Green Function (EGF) method (Hartzell 1978; Irikura 1983), (b) stochastic simulations of point or finite sources (Boore 2003; Motazedian and Atkinson 2005), and (c) deterministic three-dimensional numerical modelling.

The latter method is based on the 3D discretization of a sufficiently large portion of the earth's crust, where the equation of seismic wave propagation is solved by a suitable discrete spatio-temporal numerical approximation, thus requiring a large computational effort. However, the increase of high-performance computing resources is making more and more feasible the simulation of scenarios of future earthquakes (see e.g., Komatitsch et al. 2004; Olsen et al. 2006; Cupillard et al. 2012; Paolucci et al. 2014). This is for example the idea behind the ShakeOut experiment in California (e.g., Porter et al. 2011), where physics-based simulations of a possible M_W 7.8 earthquake on the southern segment of the San Andreas Fault were the basis to build a comprehensive earthquake risk analysis including costs evaluation and planning of emergency response activities. On the other hand, sources of uncertainty in the simulations arise from the high-frequency limit due the spatial discretization of the numerical mesh, hardly larger than 1–2 Hz, from the complexity of the earthquake source (Mai and Beroza 2002), from the insufficient detail on the geological model and from the complexity of soil response, in terms of the constitutive modelling to reproduce viscous and non-linear effects.

Nevertheless, the interest in physics-based numerical simulations does not only rely on the modeling of earthquake scenarios. Understanding how the interaction of seismic source kinematics with surface geology might have affected the uneven spatial distribution of damage during past earthquakes is an interesting field of investigation from the engineering point of view. In this framework, we present the application to the 2009 L'Aquila earthquake (central Italy), characterized by highly variable damage in the near-source region (Fig. 1) that reached the largest values of Mercalli–Cancani–Sieberg (MCS) macroseismic intensity ($I_{MCS} = 9$–10) in the villages of Onna and Castelnuovo (Locati et al. 2011).

The L'Aquila earthquake occurred at 01:32 UTC on April 6, 2009, with an estimated moment magnitude M_W 6.1 (Scognamiglio et al. 2010). The hypocenter of the event was located at around 9 km depth beneath the city of L'Aquila and the rupture activated the Paganica fault (see surface projection in Fig. 1), a $\sim 50°$ dipping and ~ 135 W trending normal fault (Chiarabba et al. 2009). The main event occurred at the end of a seismic sequence that started in January 2009 and culminated with a M_W 4 event on March 30 (13:38 UTC). After the mainshock, almost 2500 aftershocks with local magnitude $M_L > 2$ were observed and located within a 15 km thick upper crust during 2009 (Chiaraluce et al. 2011). The stress drop of the main event was estimated to be 8–9 MPa (Bindi et al. 2009; Del Gaudio et al. 2015), which is significantly larger than the average stress drop (~ 3 MPa) from foreshocks and aftershocks. This is connected with the concentration of high slip in small size patches on the fault plane (Cirella et al. 2012). The strong motion data recorded in the near-source region exhibit large amplitudes, localized peaks and large spatial variability, this latter being also observed in the pattern of the damage distribution

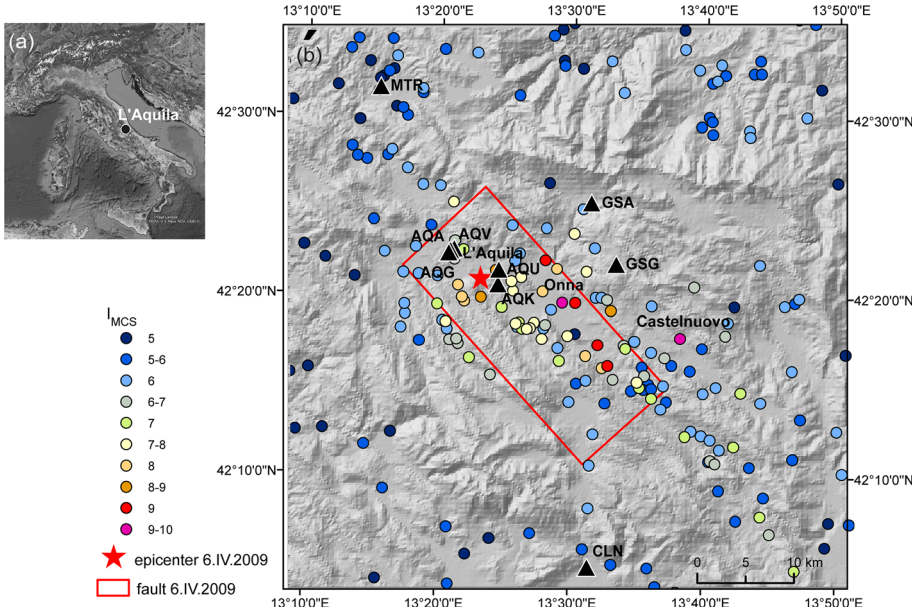

Fig. 1 The L'Aquila earthquake: **a** geographical localization; **b** I_{MCS} distribution (Locati et al. 2011), epicenter, surface projection of the fault and strong motion stations (*triangle*) of the National Accelerometric Network (RAN)

(Fig. 1). While the prevailing spatial extension of damage towards South-East (S-E) direction is attributed by some researchers possibly to the combined effect of source directivity (Chioccarelli and Iervolino 2010) and the soft sediments of the Aterno river valley (Monaco et al. 2012), local geological conditions have further enhanced the consequences of the earthquake, such as in the villages of Onna and Castelnuovo.

The objective of this paper is twofold. First, we aim at introducing the most updated investigations, both on the geological and geophysical characterization of the Aterno river valley (Sect. 2) and on the source mechanism of the 2009 earthquake (Sect. 3), to carry out 3D physics-based numerical simulations, with special emphasis on the combined effect of the source kinematics and basin configuration (Sect. 4). This is expected to improve results from past studies regarding the L'Aquila earthquake (Smerzini and Villani 2012; Magnoni et al. 2014) which did not benefit from a similar level of knowledge. For the simulations we used the numerical code SPEED (Spectral Elements in Elastodynamics with Discontinuous Galerkin, http://speed.mox.polimi.it/), developed at Politecnico di Milano (Mazzieri et al. 2013) and designed for the simulation of seismic wave propagation problems at both local and regional scales, including the kinematic modelling of seismic ruptures and the seismic wave propagation through highly heterogeneous and complex earth structures.

As a second objective, we will show how the results of physics-based numerical simulations can be used to define a physics-based input for engineering analyses (e.g., seismic site response). For this purpose, we selected the site of Castelnuovo, a small village settled on a hill with an approximate elliptical shape in plan, South-East of the Aterno river valley, where the local MCS intensity was three degrees larger than the surrounding villages (Fig. 1). Unfortunately, no record in the vicinity of the site was available, in order to shed light on the reasons of such a major impact.

A 2D finite difference model of the area of Castelnuovo was constructed for site-specific response analyses, using as input motion the broadband time histories generated through a hybrid method combining the 3D waveforms produced by SPEED at low frequency with synthetics provided by a stochastic approach at high frequency (Sect. 5). Results were compared with those obtained considering an alternative selection of input motion, achieved by deconvolution to the bedrock of the time history recorded at an accelerometric station close to the epicenter (AQG, see Fig. 1) by accounting for the amplitude decay to the site of Castelnuovo. The results of the numerical analysis are finally discussed in terms of time-histories, pseudo-acceleration spectra and amplification factor of peak ground acceleration and response spectral ordinates at periods of 0.5, 1 and 2 s.

2 Geological model of the Aterno river basin

The Aterno river valley is one of the largest intra-mountain basins of central Italy. Like other important Apennine structural depressions, such as the Fucino and Sulmona basins, it is elongated along important, North-West/South-East oriented, regional faults, which were active since the late Pliocene up to Holocene age (Galadini and Galli 2000).

The valley is bounded by high (2000 m a.s.l.) Meso-Cenozoic carbonate massifs, which show slope-to-basin facies in the northern sector and platform domains in the southern one. During the late Miocene/early Pliocene the Mesozoic dolostones, calcareous rocks and Miocenic terrigeneus flysch were interested by compressive deformations (thrusts and fold structures). Only during the late Pliocene and the Pleistocene the extensional tectonics affected the study area causing the formation of a very deep depression which was progressively filled in by clastic deposits (gravel, silt and sands). A geological map and some representative cross-sections of the middle Aterno river valley are illustrated in Figs. 2 and 3. Quaternary continental deposits are present also along the carbonate slopes and consist especially of debris and calcareous breccias, locally with intercalation of ancient pyroclastic levels (Giaccio et al. 2012; Mancini et al. 2012; Tallini et al. 2012).

Santo et al. (2014) reconstructed the subsurface geological model of the middle Aterno valley by re-interpretation of overall information from boreholes stratigraphy and from geophysics (APAT 2006; Blumetti et al. 2002; Bosi and Bertini 1970; Ge.Mi.Na 1963; Working Group MS-AQ 2010; Improta et al. 2012).

The proposed subsurface geological model points to the occurrence of five main depocentral areas, located in the North-West (N-W), central and South-East (S-E) parts of the middle Aterno valley (Fig. 4). These are respectively located South-West (S-W) of L'Aquila (inferred maximum bedrock depth around 350–400 m; orientation N150), West of the Bazzano and Monticchio carbonate ridges (maximum depth around 350–400 m; orientation N90), in the middle part of the Paganica–San Demetrio basin (depth around 250–300 m; orientation N150), in the S-E part of such basin (San Demetrio area; estimated maximum bedrock depth >550 m; orientation N50), and, finally, S-W of Barisciano, in the Castelnuovo-Civitaretenga basin (again estimated maximum bedrock depth >550 m; orientation N120).

The buried bedrock morphology only partly mirrors the spatial distribution of the present-day topographic peaks and valleys. In fact, while the depocenter in the middle Paganica–San Demetrio basin develops in the subsurface of the present-day alluvial basin, very thick (≥400/500 m) sedimentary bodies identified in the N-W and S-E parts of the

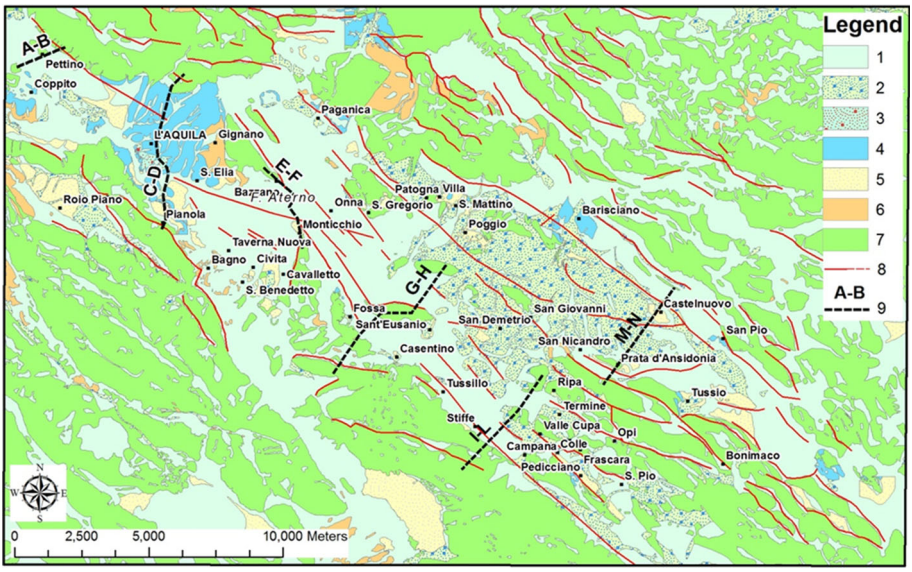

Fig. 2 Geological sketch of middle Aterno river valley (modified APAT 2006) and traces of cross-sections shown in Fig. 3. Lithology legend. Holocene deposits: *1*—Eluvio-colluvial, recent alluvial and detrital talus deposits; Pleistocene deposits: *2*—terraced alluvial poor to well-cemented calcareous gravels, ancient alluvial sands and fan; *3*—red silt; *4*—variably-cemented calcareous breccias and dense calcareous gravels; *5*—ancient silty sand and silty clay deposits; *6*—Miocene arenaceous-pelitic bedrock; *7*—Mesozoic calcareous bedrock; *8*—reactivated fault, dashed if presumed

middle Aterno valley overlap topographic highs interposed between the modern alluvial/lacustrine plains (see Fig. 4). Outcropping units, in such highs, are relatively old—lower to middle Pleistocene—alluvial/lacustrine successions. Overall evidence testifies important changes in the perimeter of the depocentral areas in the middle Aterno valley over the early Pleistocene to present time.

A shear wave velocity model of the Aterno basin was also defined through the collection and interpretation of geophysical and geotechnical investigations carried out in the area for other purposes (Santucci de Magistris et al. 2013). Based on these studies, the geological complexity of the quaternary formations filling the basin was simplified to provide a characteristic shear wave velocity,V_S, profile for each of the five depocenters.

In the perspective of 3D numerical simulations performed in this work, the seismic wave propagation model was further simplified in order to be managed by SPEED; to this end, the alluvial soils were assumed to behave as a linear viscoelastic medium, characterized by a homogeneous profile in terms of soil density, ρ, while V_S increases from a minimum value of 300 m/s at surface, following a power function with depth. The compression wave velocity, V_P, and the attenuation quality factor, Q_S, were derived as a function of the V_S profile. The parameters of the wave propagation model inside the basin are summarized in Eqs. (1–3), where z denotes the depth measured in meters.

$$\rho = 1.9\,(\mathrm{g/cm^3}) \tag{1}$$

$$V_S = 300 + 36 \cdot z^{0.43} \quad \text{and} \quad V_P = 4.57^{0.5} \cdot V_S\,(\mathrm{m/s}) \tag{2}$$

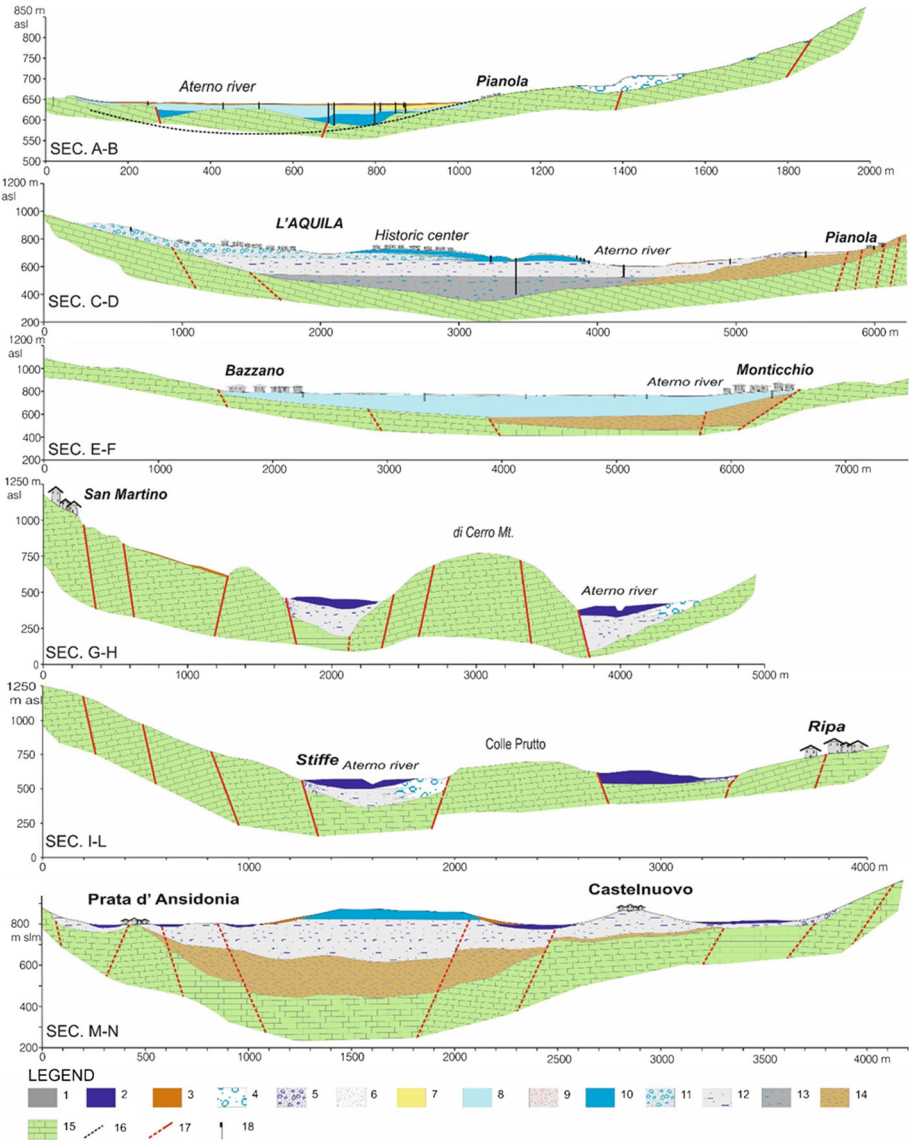

Fig. 3 Geological cross-sections of the middle Aterno river valley. Lithology legend. Holocene–Pleistocene deposits: *1*—landfill; *2*—alluvial deposits; *3*—soil and eluvio-collivial deposits; *4*—alluvial fan deposits; *5*—talus and calcareous breccias; *6*—sand and silt; *7*—silt and clay with intercalated gravel lens; *8*—gravel with a sandy matrix; *9*—red silts; *10*—silty gravels; *11*—variably-cemented calcareous breccias and dense calcareous gravels (Aquila Breccias); *12*—ancient silty sand and silty clay deposits; *13*—ancient lacustrine deposits with lignite; *14*—Miocene arenaceous-pelitic bedrock; *15*—Mesozoic calcareous bedrock; *16*—bedrock limit reconstructed by gravimetric surveys; *17*—fault, dashed if presumed; *18*—borehole

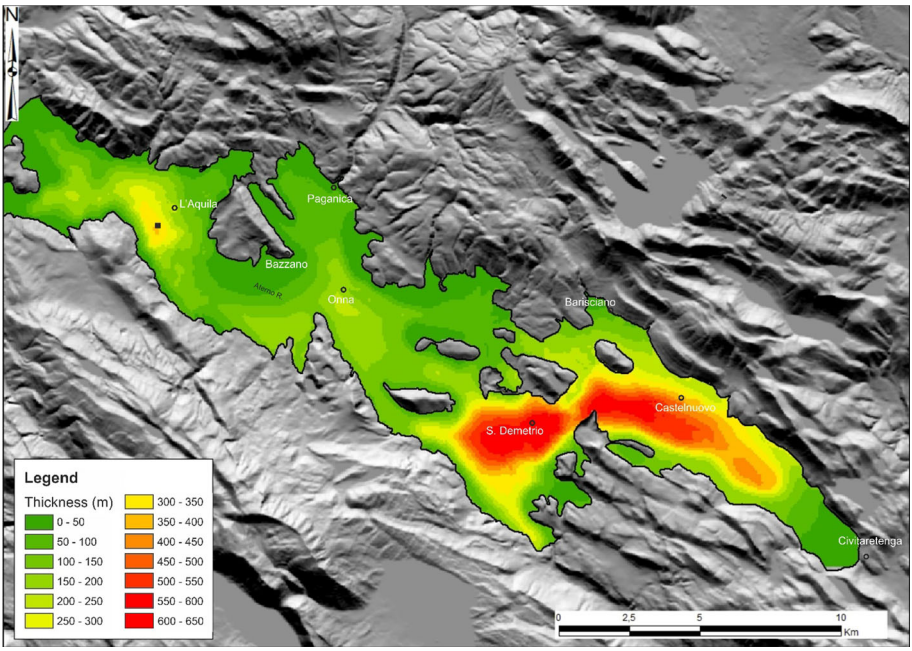

Fig. 4 Reconstruction of the thickness of Quaternary continental deposits, derived by subtracting the 40 m Digital Terrain Model (DTM) representing the distribution of the carbonate bedrock in the middle Aterno valley from the actual topography of the area (Santo et al. 2014)

$$Q_S = V_S/10 \quad \text{with} \quad V_S \text{ in m/s} \tag{3}$$

A crustal model, characterized by four horizontal layers up to a maximum depth of 20 km, as suggested by Bianchi el al. (2010) and modified by Ameri et al. (2012), was adopted to describe the rock materials beneath and outside the boundaries of the Aterno river valley. The properties of each layer of the crustal model are shown in Table 1. The V_S value of the uppermost layer, corresponding to the outcropping bedrock, was reduced to a value of 1700 m/s, according to the results of site investigations (Working Group MS-AQ 2010). This low-velocity upper layer also limits the impedance contrast with the quaternary sediments.

Table 1 Horizontally stratified crustal model assumed for the 3D numerical simulations. The columns describe the depth of the layer, the S- and P-wave velocities, the soil density and the attenuation quality factor

H (m)	V_S (m/s)	V_P (m/s)	ρ (g/cm^3)	Q_S
1000	1700	3160	2.50	100
2000	2600	4830	2.84	200
5000	3100	5760	2.94	200
20000	3500	6510	3.18	200

3 Kinematic source model of the L'Aquila 2009 mainshock

To represent the rupture process of the L'Aquila earthquake a kinematic description was adopted. We fixed the fault plane and the focal mechanism (strike 133°, dip 54°, rake 102°) of the earthquake as determined by Chiaraluce et al. (2011) and the maximum size of the fault to 28 km by 20 km, this latter containing most of the kinematic models retrieved for this event. Although several kinematic models were presented in literature during last years to describe the source process of L'Aquila earthquake, we only focused on those obtained from inversion of seismic data, which contain information on the observed strong ground motion.

Specifically, we tested three different models, namely those proposed by Cirella et al. (2012), Ameri et al. (2012) and Del Gaudio et al. (2015), hereafter indicated as CI, AM and DG respectively. This choice was related to the availability of a complete description of the rupture process. It is worth to note that other kinematic models also achieved from inversion of strong motion data, are available in literature (e.g., Poiata et al. 2012; Gallovic et al. 2015). In Fig. 5 the three kinematic models are shown in terms of slip distribution with overlapped rupture time isolines.

The models show some similarities in the slip distribution, but also significant differences. The CI model is characterized by an initial up-dip rupture propagation with a high rupture velocity ($\sim$3.5–4.0 km/s). When approaching the free surface, the rupture also starts to propagate along the fault strike direction. This model has two main slip asperities: the first one located nearly 2 km up-dip from the hypocenter and the second one southward the hypocenter and activated 2–3 s later, providing a final M_W 6.1. This model was derived from inversion of low frequency ground motion records (up to 0.3 Hz), but it naturally contains some energy at higher frequency, related to the selected parametrization for slip, rupture velocity and rise time. The DG model was also obtained from inversion of low-frequency seismic data but using a nested strategy in the frequency domain and a bi-dimensional Gaussian parameterization for the slip (Lucca et al. 2012). This model shows similar slip and rupture velocity values as the CI model (M_W 6.2), with larger size slip asperities, smaller maximum amplitude and almost same activation timing. Nevertheless, because of the Gaussian parametrization, the emitted energy spectrum exponentially decreases beyond the corner wavenumber of the Gaussian function, depleting the seismograms of high frequencies. Finally, the AM model was obtained by a combination of a low frequency kinematic inversion (Gallovic and Zaharadnik 2011) and a k^{-2} high-frequency technique (Gallovic and Brokesová 2008), with a trial and error adjustment of the kinematic parameters, to fit the amplitude and the duration of strong motion data. This model provided an M_W 6.2. Unlike the previous two models, AM rupture description naturally contains a physical description of the high frequency energy radiated from the fault.

To select the best kinematic model, synthetic seismograms were computed using a 1D velocity model in the frequency range 0.05–2 Hz. Simulations were performed using the discrete wavenumber method implemented in the code AXITRA (Coutant 1994). Green's functions were computed in the 1D model of Bianchi et al. (2010) modified by Ameri et al. (2012) and summarized in Table 1. To introduce a larger complexity in the slip description at intermediate to high frequencies, we used a variable rise time randomly distributed on the fault between 0.6 and 0.8 s.

For the model selection, the time series and the amplitude Fourier spectra of the simulated three-component (E-W, N-S and Z, which is the vertical) ground velocities

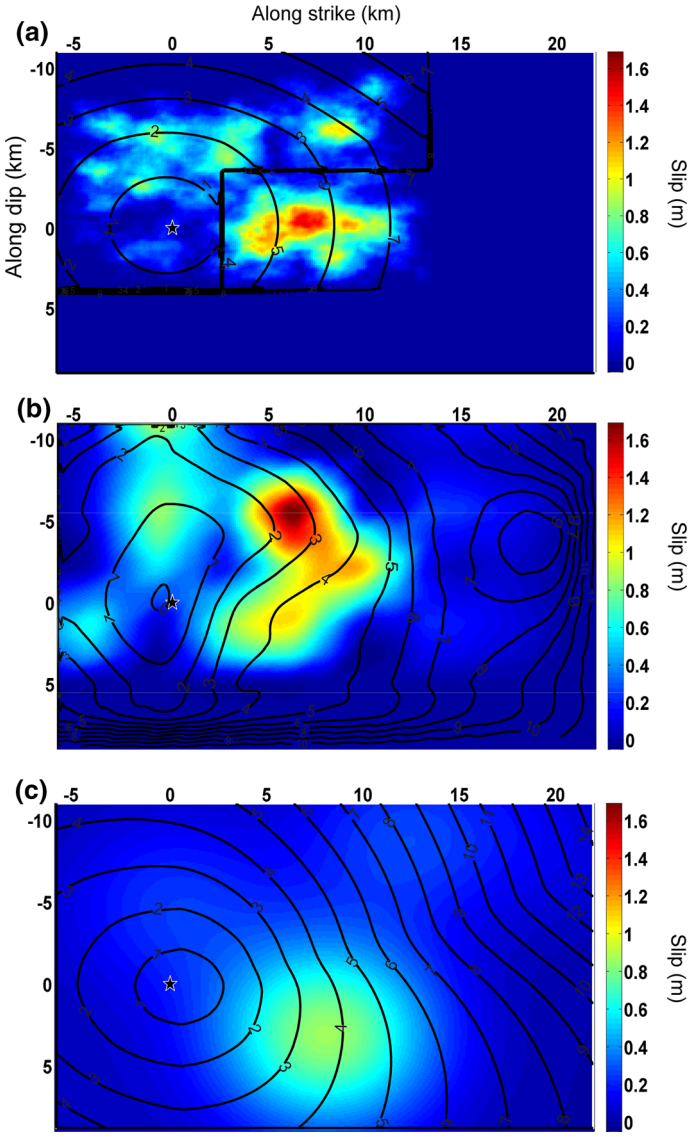

Fig. 5 Slip map and rupture time isolines of the kinematic models obtained for l'Aquila earthquake by **a** Ameri et al. (2012)**, b** Cirella et al. (2012) and **c** Del Gaudio et al. (2015)

were compared with the real observations at near-source stations. Because of the 1D approximation, we do not expect to well describe the whole signal and in this analysis, we mostly focused on the first, most energetic seismic phase. While for far-source stations the low frequency amplitude and the shape of the direct phases are comparable to real observations, as indicated by the misfit used in the inversion, the models show a different behavior for the near-source stations located in the city of L'Aquila. As an example, in Fig. 6 we presented a comparison at the stations AQG and AQU that are located within the surface projection of the fault (Fig. 1). The station AQG is located

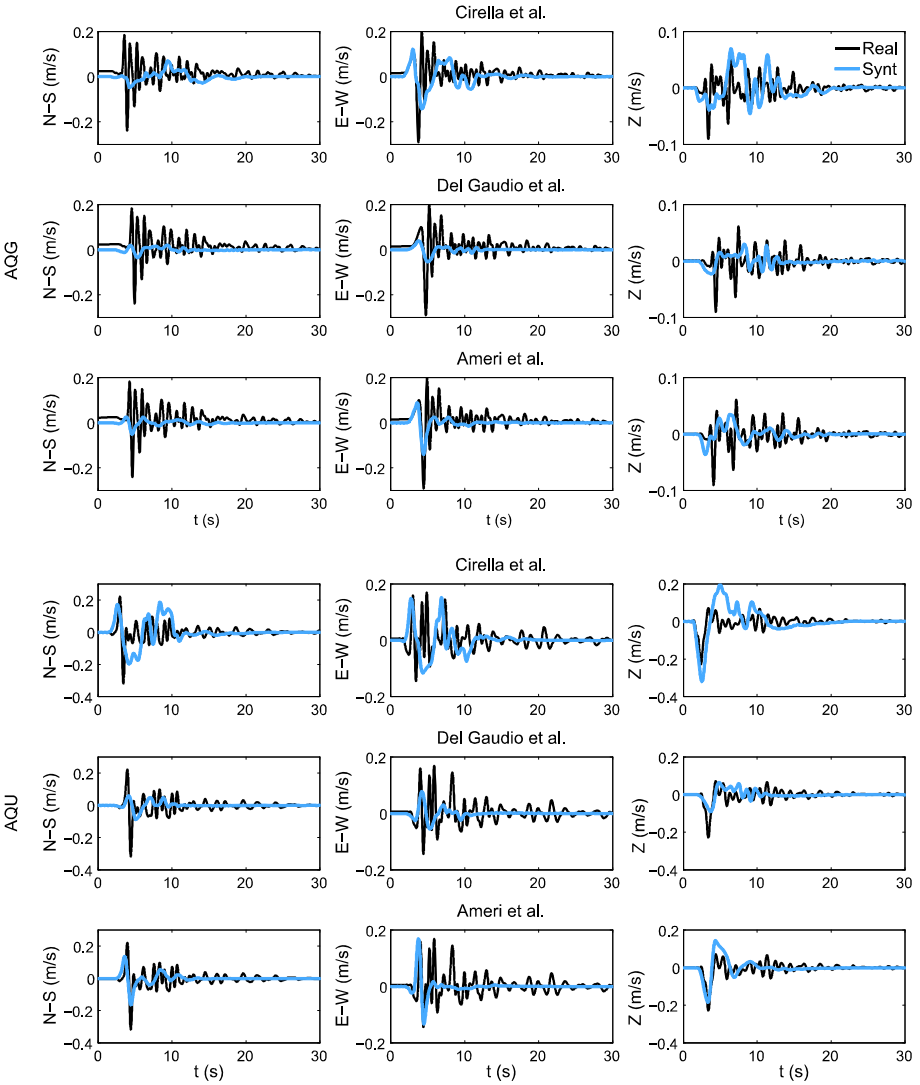

Fig. 6 Comparison between synthetic ground motion velocity (*cyan*) at the AQG and AQU stations computed with the three different models considered in this study and real observations (*black*). The synthetic signals are computed in the frequency range [0.05–2] Hz

at ∼4 km of epicentral distance, along the SW-NE cross-section of the Aterno valley, while AQU is located right in the middle of the valley, at ∼2 km of epicentral distance. For these stations, the best results were obtained with the AM model, which is able to reproduce the duration, timing and amplitude of the velocity pulse at least on one of the horizontal components. The AM fit improves for the two stations (AQU and AQK) located in the city center, where the maximum amplitude is also well reproduced on the vertical component and the shape and the duration of the impulse signal is well retrieved at the three components. For this reason, we decided to use the AM for the 3D modelling illustrated in the following sections.

4 Numerical simulation of 2009 Aquila earthquake

The 3D numerical model of the L'Aquila basin extends for 58 km in the N-S and E-W directions with a maximum depth of 20 km, as constrained by the size of the fault (Fig. 7 a). The geometrical model was built by overlapping the topographic layer, obtained by a 250 m resolution digital elevation model, with the layers describing the bedrock morphology and including the fault geometry, as described in the previous sections.

The numerical domain was discretized to provide a mesh of 3×10^5 hexahedral elements (Fig. 7b). The size of the elements ranges from a minimum of 133 m, within the quaternary basin, up to 400 m in the outcropping bedrock. The mesh was generated to propagate up to about 2 Hz for a spectral degree 3; the time step for the explicit second-order finite difference integration scheme was set to Δt equal to 10^{-3} s for a simulated time of 30 s. The simulations were performed on the computing cluster of the University of Naples Federico II (i.e., SCOPE; http://www.scope.unina.it/) using 132 parallel CPUs, resulting in a total computation time of about three hours for a single scenario.

The 3D numerical simulations were carried out assuming the AM source model, as described in Sect. 3. In Fig. 8 the contours of the snapshots of the E-W velocity wavefield at 6, 10, 16 and 20 s are displayed, showing that the numerical model well reproduces the up-dip rupture propagation and a wave focalization within the basin, particularly in the location of the deepest depocenters.

The numerical results are then compared with the records of the mainshock in terms of velocity time histories and velocity Fourier spectra at three selected recording stations of the RAN seismic network (Fig. 1). To properly compare the observed and simulated data, the waveforms were processed with a band-pass Butterworth filter between 0.1 and 2 Hz, according to the maximum frequency propagated by the 3D model. Figure 9 shows the comparison between numerical and observed signals at the near-source stations AQU, AQG and AQK, in terms of three component velocity time histories (Fig. 9a) and corresponding Fourier amplitude spectra (Fig. 9b). For the same rupture scenario, we represent the results obtained by 1D (AXITRA) and 3D simulations (SPEED), plotted with cyan and red curves, respectively. Note that both 1D and 3D simulations include the same extended kinematic source model (AM model) but they differ for the subsoil horizontally layered

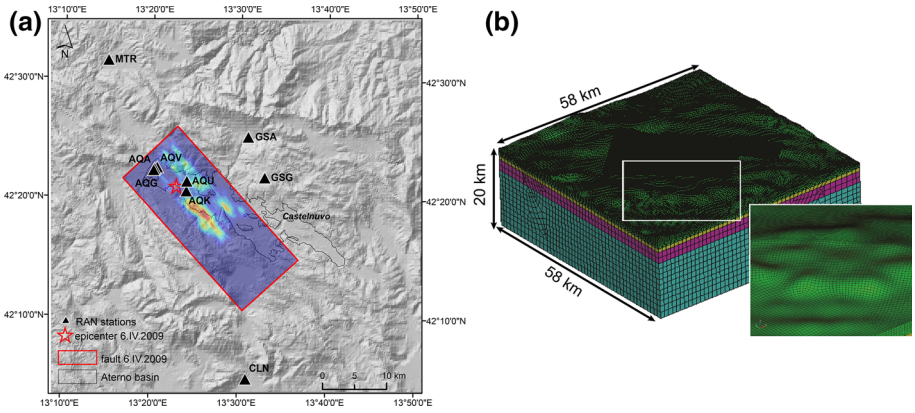

Fig. 7 3D model of the L'Aquila basin: **a** extension of the computational domain and slip distribution, **b** numerical mesh consisting of 3×10^5 hexahedral elements

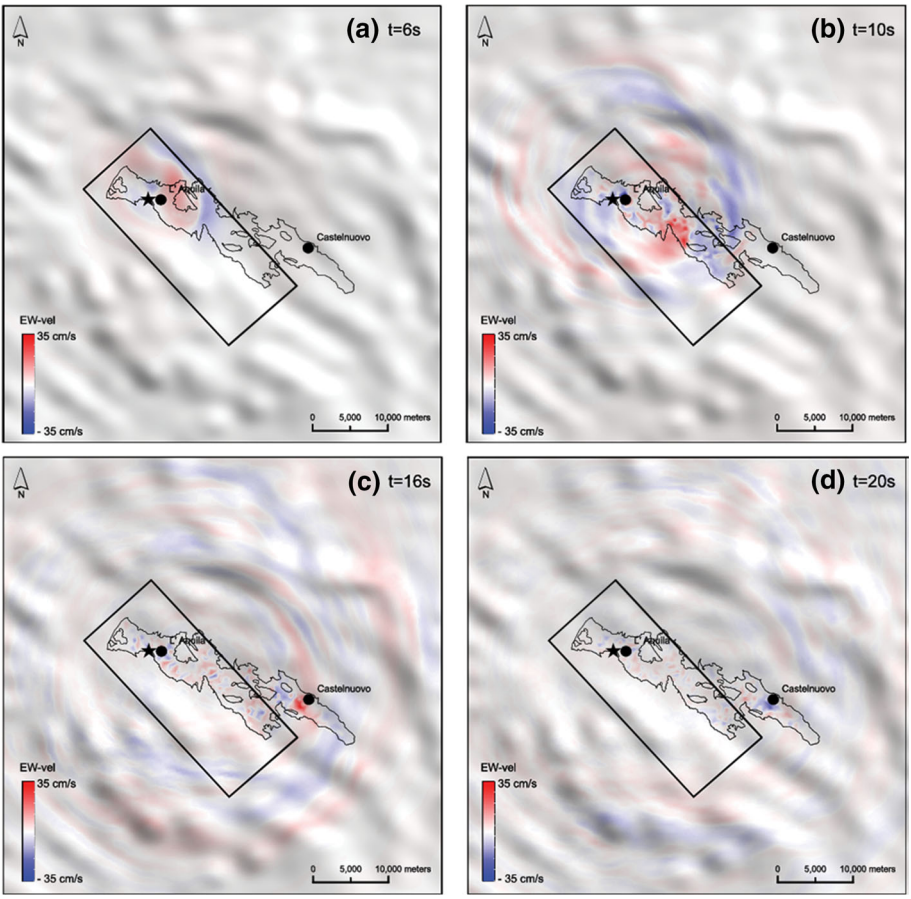

Fig. 8 Contours of E-W velocity at **a** 6 s, **b** 10 s, **c** 16 s and **d** 20 s (download animations at http://wpage.unina.it/iuniervo/EW3.wmv and http://wpage.unina.it/iuniervo/NS3.wmv)

rock structure without the presence of the basin for the former model and with the 3D geological description of the Aterno river valley for the latter one.

Comparing the two simulations, we observe similarity in the spectral behaviour and high-frequency decay. In the time domain, instead, 1D simulations only capture the main initial phase of the records and rapidly decay to zero, as compared to both real data and 3D simulations. For several stations, they consistently catch the peak amplitude, but significantly underestimate the duration and the energy distribution with time. For 3D simulations, we obtain a good correspondence in the energy distribution with time at least for synthetics at AQU and AQK, which are located in the central part of the city of L'Aquila, and southward of the epicenter. At these two stations, the observed velocity on the three components is well reproduced by synthetics. Simulations also describe the impulsive contribution with duration of about 1 s at the beginning of the signal and consistently the peak ground velocity (PGV). For these stations, also the Fourier velocity spectra are well represented up to 1 Hz. A significant decrease of the spectral amplitude is clearly observable between 1 and 2 Hz, which is not present in the data, indicating that fine details

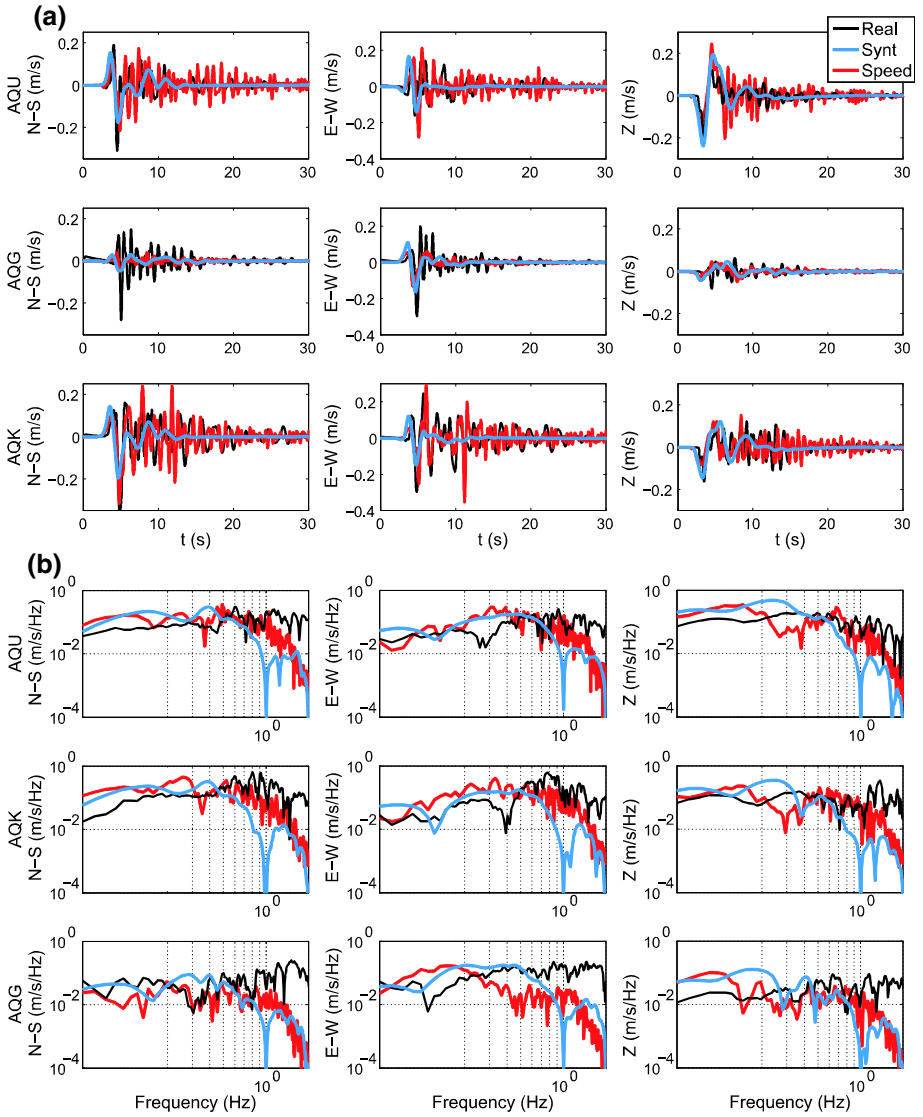

Fig. 9 Comparison between numerical results (*cyan* by AXITRA and *red* by SPEED) and records (*black*) at stations AQU, AQG and AQK: **a** velocity time history; **b** Fourier spectral amplitude. The numerical results by AXITRA are computed in the frequency range [0.05–2] Hz

of the velocity model or the source rupture may have played a significant role in this frequency range.

At the station AQG, instead, the synthetic time series underestimate the amplitude of the real signal on two of the three components. Specifically, the amplification of the impulsive peak on the velocity is only partially captured on the E-W component, but is missing on both the N-S and Z components. The discrepancy in the data fitting could be attributed to a source effect, indicating a possible small-scale up-dip asperity, north of the hypocenter and/or as a site effect. De facto, in the numerical model this station is assumed to lie on

outcropping bedrock ($V_S = 1700$ m/s), while in the reality the station is located on a weathered and fractured limestone deposit, which is characterized by a shear wave velocity profile corresponding to a relatively stiff soil site on the basis of the average shear wave velocity in the top 30 m, V_{S30} (Lanzo et al. 2011b). Referring to the Fourier spectral amplitude the same behavior as for the AQU and AQK stations is found, with an acceptable representation of spectrum up to 1 Hz and a faster decay in the synthetics beyond this frequency.

To highlight the spatial variability pattern of ground motion as predicted by the 3D numerical model, Figs. 10 and 11 show the maps of PGV and response spectral displacement (SD) at the vibration period T = 3 s, respectively, for both the horizontal components normal and parallel to the fault strike, denoted by FN (a) and FP (b), respectively. On the same maps, the simulated velocity (Fig. 10) and displacement (Fig. 11) time histories at selected locations (AQG, AQK, GSA, Paganica, Onna, Castelnuovo; see Fig. 1) are superimposed to shed light on the variability of seismic motion in time. Furthermore, the observed values of MCS intensity greater than 8 are also indicated.

We can observe that: (1) the FN component reaches a maximum PGV of about 50 cm/s, 70% higher than the maximum PGV on the FP component (about 30 cm/s); (2) the maximum SD is about 30 cm on both the FN and FP components; (3) the contour maps in Fig. 11 show that the long-period spectral displacement, SD (T = 3 s), especially on the FN component, is significantly amplified at the location of the main depocenters. Since a significant energy contribution at 3 s is also present along the rock outcrop outside the basin, especially in the area North of Castelnuovo, as highlighted in Fig. 11b, we may argue that such amplification is likely due to the coupling of the radiation pattern of the seismic source and possible up-dip directivity effects as suggested by Tinti et al. (2014), with deep basin wave interaction; (4) in perspective of the ground response analyses which will be shown in the following section, it is worth highlighting that the configuration of the S-E portion of the Aterno valley (i.e., the Castelnuovo-Civitaretenga basin) with maximum bedrock depth larger than 550 m, impacts on ground motion amplification at long periods;

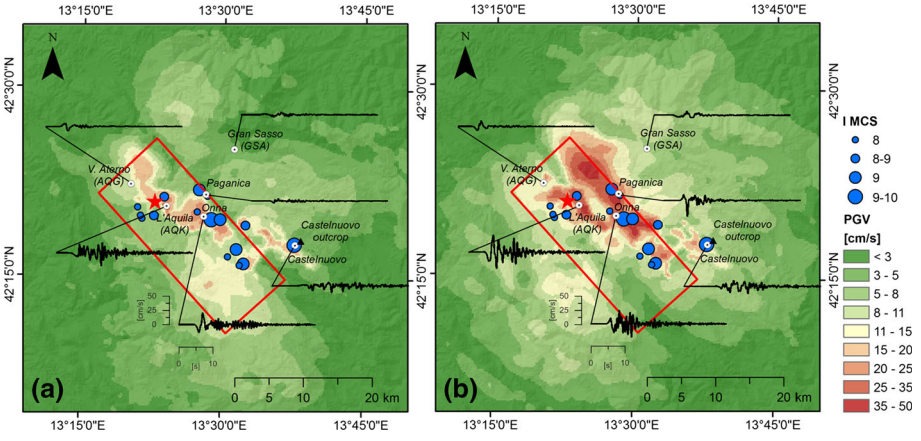

Fig. 10 PGV map for the **a** FP and **b** FN components, together with the corresponding velocity time histories at selected sites (AQG, AQK, GSA, Paganica, Onna, Castelnuovo) and the observed values of MCS intensity greater than 8 (*dots*). The location of the receiver at Castelnuovo on outcropping bedrock adopted as input motion for the seismic response analysis (*triangle*) is also indicated

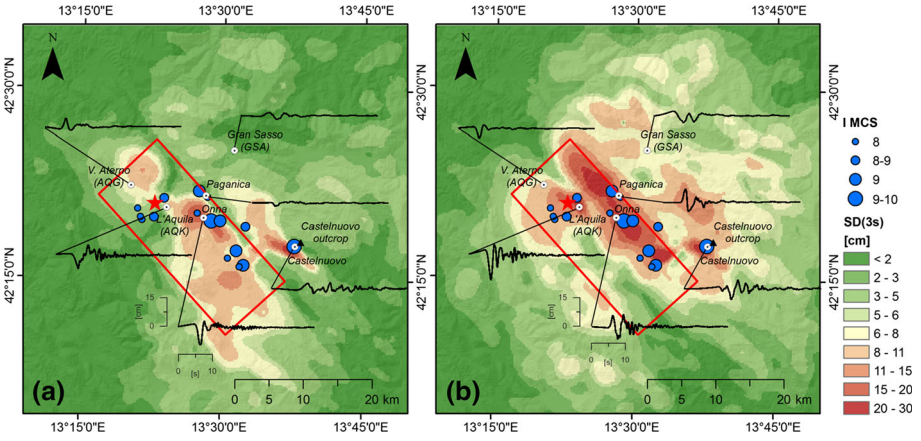

Fig. 11 Map of the spectral displacement at 3 s (SD at T = 3 s) for the **a** FP and **b** FN components, together with the corresponding displacement time histories at selected sites (AQG, AQK, GSA, Paganica, Onna, Castelnuovo) and the observed values of MCS intensity greater than 8 (*dots*). The location of the receiver at Castelnuovo on outcropping bedrock adopted as input motion for the seismic response analysis (*triangle*) is also indicated

(5) the spatial distribution of FN-PGV is related to the assumed kinematic finite-fault model, in particular with both the hypocenter location and the slip pattern (see Fig. 7); (6) the comparison between the spatial variability of simulated ground motion (i.e., PGV and SD at T = 3 s) and the distribution of the observed MCS intensity shows a satisfactory agreement on the FN component. The intensity and the ground motion parameters take their highest values in the N-W/S-E direction. In particular, it is interesting to note that the maximum value of SD (T = 3 s) is reached at the sites of Paganica, Onna end Castelnuovo, where I_{MCS} = 9–10 was observed.

The comparison between observations and synthetics for the eight stations close to the fault is summarized in Fig. 12a, b in terms of Goodness-of-Fit (GoF) scores (Anderson, 2004). For each monitored RAN stations, the GoF scores of Arias Intensity (AI), Energy Intensity (EIM), PGV, peak ground displacement (PGD), Response Spectra (RS), Fourier amplitude spectrum (FS) and Housner Intensity (SI computed between 0.5 and 2 s) are

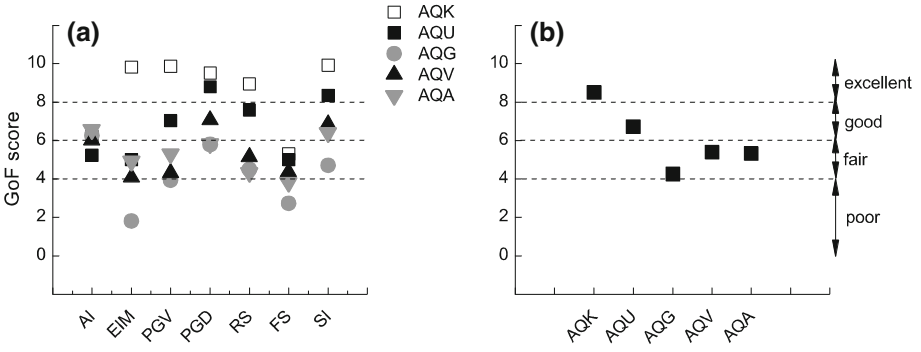

Fig. 12 Goodness-fit-scores in the frequency band between 0.1 and 2 Hz: **a** for the five monitored stations; **b** average values of the seven metrics for each stations

evaluated in the bandwidth 0.1–2 Hz. For each station, the scores of the seven metrics are assessed as the average of the values associated with the three components.

The results show a misfit between recorded and numerical waveforms especially in the Fourier amplitude spectrum and EIM (Fig. 12a). This underestimation is likely due to a combination of the simplified model adopted for the deposits filling the basin and the lack of high-frequency energy content in the source model. The overall comparison (Fig. 12b), in any case, provides a fair to good GoF for the investigated stations, with the overall score decreasing with the distance from the source.

5 Seismic response analysis at Castelnuovo

As already pointed out in the introduction, the numerical simulation of the 2009 L'Aquila earthquake can help to define a physically constrained input motion for seismic response analyses at sites where accelerometric records are not available. This is the case of the village of Castelnuovo, where it was sought to better understand how the interaction of seismic source kinematics with surface geology may have affected the local ground motion and the observed uneven spatial distribution of damage. Therefore, 2D seismic response analyses of the Castelnuovo hill were carried out by considering the following reference input motions:

1. the broadband signals obtained by combining the 3D synthetics simulated at low frequencies by SPEED at an outcropping site near Castelnuovo (see filled triangle in Figs. 10, 11), with high-frequency synthetics generated by an independent stochastic method;
2. the signal recorded at AQG station during the mainshock, after deconvolution to the bedrock and amplitude scaling accounting for the source-site distance.

Further details about the procedure followed to generate input motions (1) and (2) will be provided in Sect. 5.1. The subsoil morphology and the mechanical properties of the Castelnuovo hill were defined on the basis of available geophysical and geotechnical investigations, as illustrated in Sect. 5.2. Based on this model, 2D seismic response analyses along two representative cross-sections of the hill, aligned along the FN and FP directions, were carried out. The horizontal components of both synthetic (1) and recorded (2) signals, projected along the same directions of the sections, were used as reference input motions assuming vertically propagating SV waves. To perform this analysis, the commercial code FLAC2D (ITASCA 2006), based on the Finite Difference Method (FDM), was used (see Sect. 5.3).

5.1 Reference input motions

Referring to the approach (1), the broadband input motion was obtained by combining the low-frequency (LF) waveforms obtained by SPEED with the high-frequency (HF) signals generated using the method proposed by Sabetta and Pugliese (1996), referred to as SP96 hereafter. SP96 allows for generating non-stationary artificial accelerograms, matching the median response spectrum by a Ground Motion Prediction Equation (GMPE), for a given magnitude, epicentral distance (R_e) and site conditions. In this case, M_W 6.2 and R_e equal to 22.1 km were assumed to simulate the high-frequency content of the signal on outcropping rock at Castelnuovo.

The HF and LF parts were combined using matching filters in the frequency domain, following the procedure illustrated by Smerzini and Villani (2012). For this purpose, the HF and LF parts were connected within a frequency band ranging between 0.6 and 1 Hz; a corner frequency of 0.8 Hz was selected to constrain the LF part of ground motion to the frequency range in which the fit of SPEED results with records was satisfactory. Beyond such corner frequency, the input motion is dominated by the stochastic part generated according to the SP96 approach.

The second input, denoted by AQG, was obtained as follows:

(i) the NS and EW components of the acceleration time history recorded at AQG were first deconvolved by the local 1D response of the soil, assuming the V_S profile available on the ITACA website (http://itaca.mi.ingv.it/) and a linear equivalent visco-elastic behavior of the soil (see Evangelista et al. 2016, for more details), to obtain the ground acceleration at the bedrock;

(ii) the resulting accelerograms were projected along the FP and FN directions and then scaled to a peak ground acceleration (PGA) equal to 0.11 g, that is the median estimated for the site of Castelnuovo through the GMPE proposed by Sabetta and Pugliese (1996).

Figure 13 shows the comparison between the input motions in terms of time histories of acceleration, velocity and displacement, together with the corresponding acceleration Fourier spectra, for FP and FN components. Figure 14 shows the corresponding 5% damped pseudo-acceleration response spectra, together with the median spectrum predicted (in terms of largest horizontal component) by SP96 for Castelnuovo (M_W 6.2, $R_e = 22.1$ km, rock outcrop). The time histories have similar features in the high-frequency range, but significant differences are apparent in the low-to-medium frequency ranges. The apparent lack of energy between 0.5 and 1 Hz in the Fourier spectrum, especially in the FN component (Fig. 13b), may be related to the position of the outcropping Castelnuovo site with respect to the Castelnuovo depocenter (Fig. 4). As it can be deduced by comparing the PGV map in Fig. 10 and the 3 s spectral displacement in

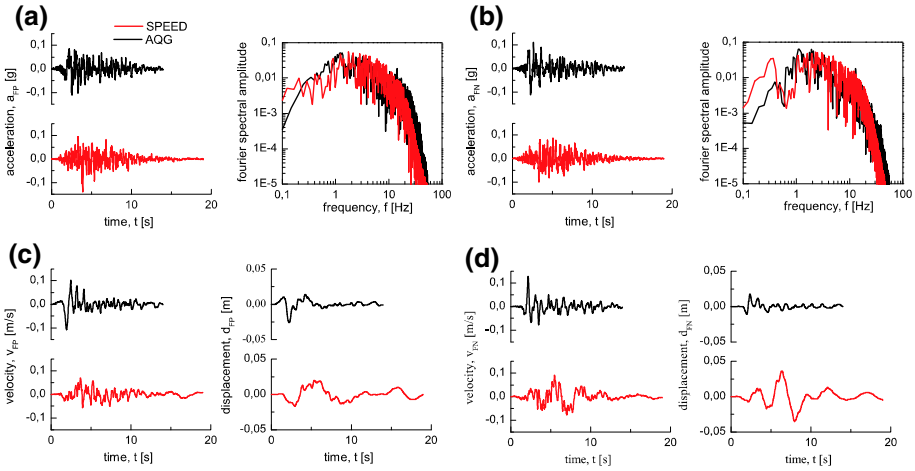

Fig. 13 Comparison between SPEED (*red*) and AQG (*black*) input motions in terms of time history (acceleration, velocity and displacement) and acceleration Fourier spectra, on the **a**, **c** FP and **b**, **d** FN components

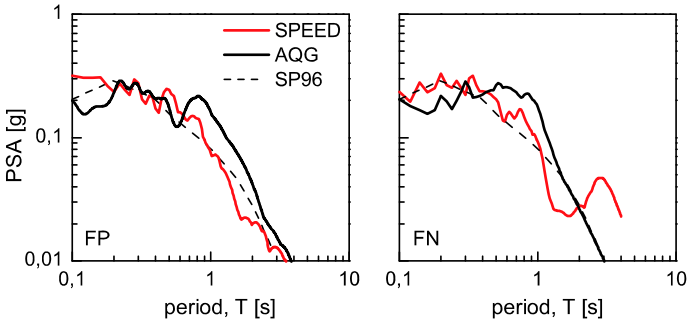

Fig. 14 Comparison of the pseudo-acceleration response spectra (PSA) of the selected input motions together with the median prediction of SP96 for Castelnuovo (M_W 6.2, R_e 22.1 km, rock outcrop)

Fig. 11, the presence of the depocenter seems to filter out the relatively high-frequency components of seismic waves, acting as a screen against seismic wave propagation beyond the basin itself. Instead, the propagation of the long period components is less affected by the presence of the basin. Besides, beyond 0.8 Hz, the approach adopted for the broadband hybrid composition, as above detailed, may also have affected the spectral content. Namely, the AQG-based input motion presents short duration and relatively large values of PGV, essentially reproducing the pulse-like features of the AQG record (Chioccarelli and Iervolino 2010), with a large spectral peak at around 1 s, clearly visible in Fig. 14. On the contrary, the SPEED-based input motion is characterized by a lower PGV and a longer duration, related to the travel path from the source to the site, with a significant peak of the FN component at around 3 s. As already argued commenting Fig. 11, this feature should be basically ascribed to combined effects of the source and wave propagation, inducing a singular concentration of long-period spectral amplitude at 3 s even at the site considered as the reference rock outcrop for Castelnuovo.

5.2 The numerical model of Castelnuovo hill

The model of Castelnuovo hill was built on the basis of the detailed geophysical and geotechnical investigations carried out during the seismic microzonation of L'Aquila basin (Working Group MS-AQ 2010; Lanzo et al. 2011a; Landolfi et al. 2014; Evangelista et al. 2016). The numerical domain has a rectangular base with sides oriented along the FP and FN directions and having a length of 700 and 600 m, respectively (Fig. 15a). The surface morphology approximates the local topography, while the bottom boundary is a horizontal plane placed 200 m under the hilltop.

The subsoil layering mainly consists of white carbonate silt, reaching a thickness of 150 m at the top of the hill. The white silt formation rests on a stratum of continental breccias, overlying a weathered layer of Miocene calcarenite that overlaps the bedrock, consisting of the same carbonate formation.

Figure 15b shows the stratigraphic sequence along central axis of the hill and the related shear wave velocity profile, together with the soil unit weight, γ, and the initial damping values, ζ^*, adopted in the model. The V_S variation with depth in the carbonate silt was obtained from the joint interpretation of the results of down-hole and resonant column tests (Evangelista et al. 2016). The underlying soft rocks were characterized using the results of geophysical tests carried out on similar soils in the Aterno valley.

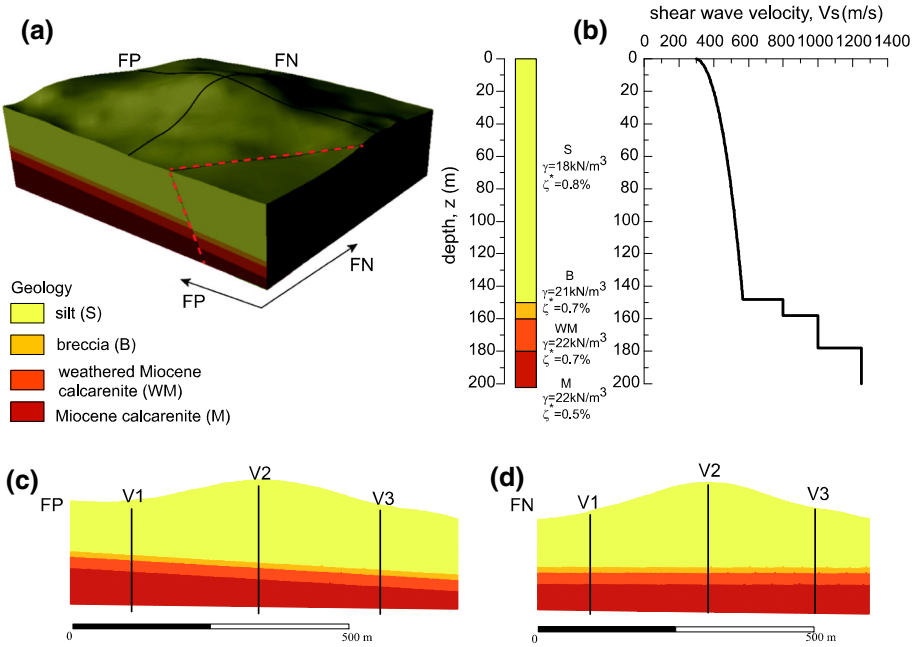

Fig. 15 **a** 3D model of Castelnuovo hill; **b** geotechnical soil model and V_S profile; **c**, **d** 2D cross-sections aligned along the FP and FN directions

All materials were modeled assuming a linear visco-elastic behavior. A frequency-dependent damping factor was adopted for the silt, modeled according to the Rayleigh formulation (Hashash and Park 2002) and following the single-frequency approach (Costanzo 2007). The damping values for the breccias and weathered and intact calcarenite were taken from the literature and assumed as frequency-independent.

Two representative sections aligned along the FP and FN directions, respectively, were extracted from the 3D model (Fig. 15a, c, d) and used for the 2D seismic wave propagation analyses. To optimize the computation time and accuracy of the simulations, the 2D models were discretized assigning a mesh size ranging between $\lambda_{min}/6$ and $\lambda_{min}/8$, being λ_{min} the minimum wavelength equal to V_S/f_{max} transmitted along a given material, according to the criteria suggested by Lysmer and Kuhlemeyer (1969). To this aim, the input signals were cut-off at 10 Hz. The domain was discretized using quadrilateral elements, imposing an average element size of about 2.5 m.

Static condition in the x and y directions was imposed at the bottom of 2D meshes, while null horizontal displacements were set at the nodes of the lateral sides, where 'free-field' dynamic boundary conditions were applied. 'Quiet boundaries' conditions were adopted at the base to avoid spurious wave reflections. The seismic motions were applied at the base nodes as a time history of the shear stress. FN and FP components were applied to the corresponding cross-sections.

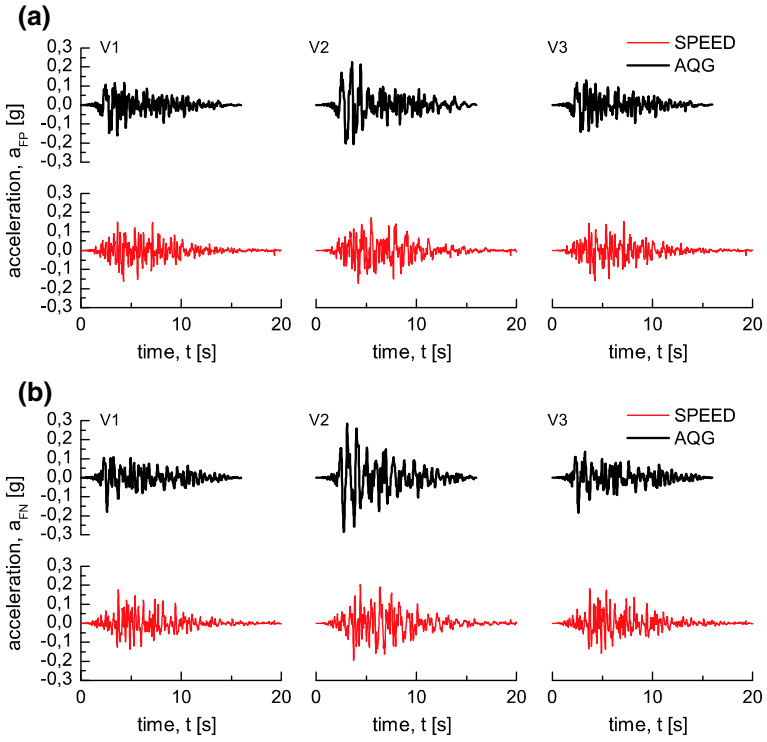

Fig. 16 Acceleration time histories at the surface of the monitored verticals for the **a** FP and **b** FN cross-sections

5.3 Numerical results

In the following, the results of the FLAC2D numerical analyses (Fig. 16) are first presented in terms of acceleration time histories obtained at the free surface of the three verticals (V1, V2 and V3) shown in Fig. 15c, d, located along the FP and FN cross-sections.

The surface ground motions resulting from the analyses carried out using SPEED and AQG inputs overall are in agreement. The results confirm the peculiar features of the seismic response of the hill, already evidenced by previous numerical analyses carried out with 2D (Lanzo et al. 2011a; Sica et al. 2013) and 3D models (Evangelista et al. 2016). Specifically, it can be noted a significant amplification of the acceleration amplitude at the hilltop (V2) that tends to decrease along the slope (V1, V3), apparently due to topographic effects. The PGA computed on the hilltop varies between 0.3 g, for the AQG input, to 0.2 g, for the SPEED input.

The differences in the results of the seismic analyses carried out with the two input motions can be better appreciated when looking at the pseudo-acceleration response spectra (PSA): Fig. 17a, b show the comparison between the spectra of the input motions and those computed at surface (denoted by 'output' in the figures) of the three monitored verticals, along the FP and FN cross-section, respectively.

The spectral shapes are significantly affected by the coupling between the adopted input motion and the dynamic response of the hill. A clear peak is recognized at 1 s on the response spectra predicted at the hilltop (V2) in both cross sections, independently of the

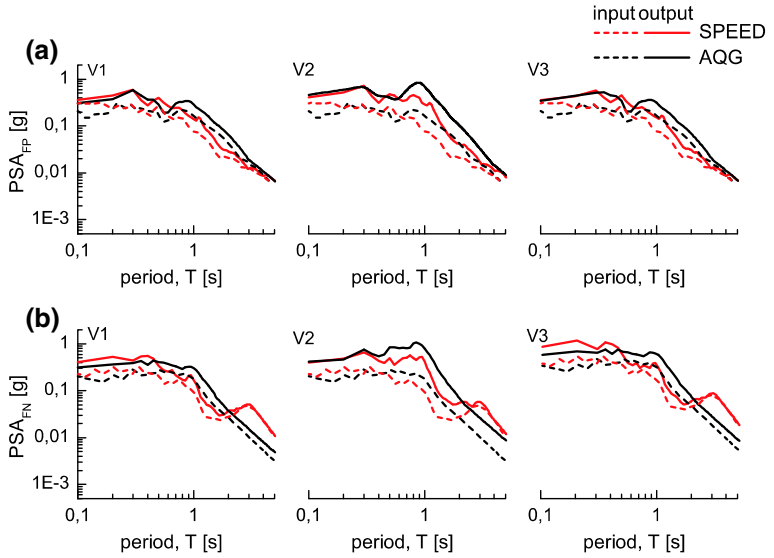

Fig. 17 Pseudo-acceleration spectra at the surface of the monitored verticals for the **a** FP and **b** FN cross-section

adopted input motion (SPEED or AQG). This period corresponds to the fundamental frequency of the entire hill, as experimentally detected by Gallipoli et al. (2013) through H/V spectral ratios obtained from noise and weak-motion records. It is also quite well captured by the above results, confirming the effectiveness of the numerical model. An apparent resonance effect at 1 s can be inferred by the response spectra obtained from the AQG motion, due to the coincidence between the frequency of the input pulse and that of the hill.

At the foot of the hill, instead, the dynamic response is expected to be mainly governed by stratigraphic effects. This is more evident at higher frequencies due to the reduced soil thickness. The dominant amplification peaks detected at around 0.4 s in the response spectra computed at the verticals V1 and V3 (Fig. 17) correspond to the second natural frequency of the relevant one-dimensional soil profiles at the foot of the hill, as confirmed by the analytical amplification functions reported by Evangelista et al. (2016). Note that, at all the verticals, the surface response to the FN component of the SPEED input motion shows a secondary spectral peak at 3 s with about the same amplitude of the reference signal, demonstrating that the long-period component was not affected by neither stratigraphic nor topographic amplification.

The results of numerical analysis are also summarized and compared in terms of amplification factors of PGA and PSA at periods T = 0.5, 1 and 2 s, referred to as F_{PGA} and F_{PSA}, respectively. The distribution of the amplification values along the two sections are plotted in Fig. 18, demonstrating a broadband amplification throughout the hill, with the maximum attained at the top, and the amplitude decreasing according to the morphology of the relief. In particular, at 1 s, the amplification factor reaches its maximum value (about 4) at the hilltop, while on the flanks it ranges between 1.5 and 2.5, independently of the input motion. At lower and higher periods, the amplification profiles are overall flatter and at the hilltop they reach peak values more comparable to those predicted at the foot of the slopes. It follows that the most significant amplification phenomena at

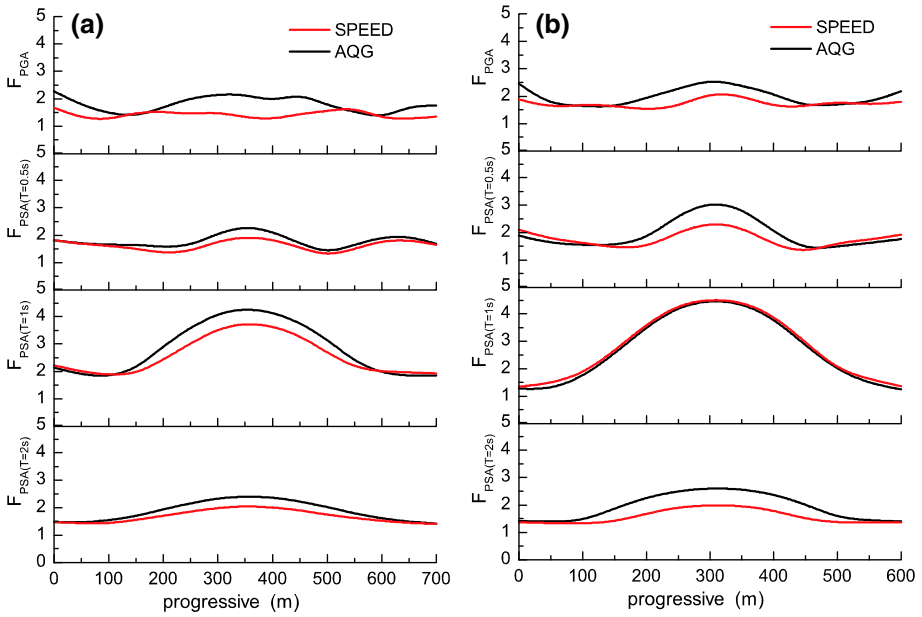

Fig. 18 Comparison of F_{PGA}, F_{PSA} at T = 0.5 s, 1 s and 2 s along cross-sections **a** FP and **b** FN

Castelnuovo should have affected the frequency components around 1 Hz, i.e., the band empirically associated to the pulse at the source, rather than the high period vibration (2–3 s), apparently introduced by the propagation along the basin.

6 Conclusion

In this study, an updated 3D physics based numerical simulation of earthquake ground motion in the Aterno river valley has been addressed first, considering, on one side, the recently acquired knowledge about the local geology, and, on the other side, the most acknowledged solutions for the slip distribution along the seismic fault. Among the source models available in literature, for which a complete description of the rupture kinematics was available, we selected the Ameri et al. (2012) description of the L'Aquila earthquake, as the best model from the velocity fit with near-source observations. Seismic waves generated by the fault rupture propagated in the crustal model and entered in the Aterno basin, which was modelled both in terms of morphology and in terms of mechanical properties of the filling sediments. It was found that as the rupture propagated southwards, the different depocenters captured the largest amplitudes in terms of velocity owing to trapped surface waves. Comparison between synthetics and observations shows, on average, a fair-to-good fit in terms of goodness of fitting parameters according to Anderson (2004). It turned out that the near-source impulse recorded at L'Aquila stations was almost retrieved on the E-W component for the stations towards the edge of the fault and on all components for mid-fault stations.

The spatial distribution of peak values of ground motion shows some agreement with the MCS intensity variability. Particularly, attention was focused on the site of Castelnuovo, a village located at the top of a hill, which, in spite of the relatively large epicentral

distance, suffered a major damage from the earthquake, up to the 9–10 degree of the I_{MCS} scale, larger than that of the surrounding villages.

The physics-based numerical simulation confirms that in the S-E side of the Aterno river basin, where the village is located, the coupling of the slip propagation along the fault with the complex shape of the Aterno basin induced a significant increase of the ground motion amplitude. However, due to inherent limitations of both source and basin models, such simulation was expected to reproduce the frequency content of the surface ground motion up to about 0.8 Hz; on the other hand, previous experimental and numerical studies showed that the maximum amplification of the hill is around 1 Hz, due to coupling of topography effects with the stratigraphic amplification related to the low impedance of the soft carbonate silt. Therefore, to provide a better insight on the possible causes of the extensive damage in Castelnuovo, we constructed a broadband seismic input, where the low-frequency range of ground motion was provided by the numerical results obtained by SPEED, as constrained by the best models of both the seismic source and of the Aterno river basin. With this hybrid input motion and that inferred by deconvolution and scaling of the near-source record, 2D numerical simulations of the seismic response of Castelnuovo hill were then carried out with FLAC 2D, on a more detailed layered subsoil model than it was possible to implement in the 3D SPEED simulations. With such a downscaling of the domains of analyses, it was possible to recognize that the extensive damage at Castelnuovo (Borghini et al. 2011; Ortolani et al. 2012) might have been related to topographic resonance phenomena around 1 Hz, as well as to additional amplification at higher frequencies, closer to those typical of the low-rise buildings of the village, as also demonstrated by the 3D analyses by Evangelista et al. (2016).

This work may contribute towards the use of 3D physics-based numerical simulations, as an alternative to real records, for determination of input motion for earthquake engineering analyses, especially when records are hardly available, such as in the near-source region of large earthquakes. However, it also pointed out some caveats that should be carefully considered in the case such 3D numerical results are used for engineering applications.

- The frequency limitation of the numerical simulations is still unavoidable, both in terms of the detailed knowledge of the geological model and of the spatial variability of the slip distribution along the fault. Recent results of a similar experiment carried out on the May 29, 2012 Po Plain earthquake, Northern Italy (Paolucci et al. 2015), have shown that some excellent fits with records may be obtained, but in a frequency range not exceeding about 1.5 Hz. In the case of the L'Aquila earthquake simulation, this range was significantly lower, up to around 0.8 Hz, because it was not possible to achieve a better constrain on the slip distribution.
- For ground motion simulation of future earthquakes in a given region, the spatial–temporal slip distribution model along the fault should be complex enough, to excite a sufficiently large range of frequencies, at least up to about 1.5 Hz. Besides, a sufficiently large number of fault slip realizations should be considered, in order to determine the event-to-event variability of ground motions at specific sites.
- More effective approaches should be devised to produce reliable broadband ground motions, by coupling the LF physics-based range with the HF stochastic range: current approaches, such as that used in this paper, fail at properly accounting for the correlation of the LF and HF ranges at a single station, but also they do not preserve the station-to-station spatial coherency of the simulated ground motions in the HF range.

Acknowledgements This work was developed within the DPC-ReLUIS Special Project RS2, on numerical simulations and near-source effects. Iunio Iervolino acknowledges the work carried out within the Ground Motion Simulation Validation (GMSV) technical activity group (TAG) of the Southern-California Earthquake Center (SCEC). All the authors gratefully acknowledge the working group of the SCOPE data center (University of Naples Federico II) for their fundamental contribution to computations.

References

Ameri G, Gallovic F, Pacor F (2012) Complexity of the Mw 6 3 2009 L'Aquila (central Italy) earthquake: 2 Broadband strong motion modeling. J Geophys Res 117:B04308

Anderson J (2004) Quantitative measure of the goodness-of-fit of synthetic seismograms. In: Proceedings of the 13th world conference on earthquake engineering, Vancouver, paper 243

APAT (2006) Carta geologica d'Italia alla scala 1:50,000, Foglio 359 "L'Aquila" APAT-Servizio Geologico d'Italia and Regione Abruzzo

Bianchi I, Chiarabba C, Piana Agostinetti N (2010) Control of the 2009 L'Aquila earthquake, central Italy, by a high-velocity structure: a receiver function study. J Geophys Res 115:B12326

Bindi D, Pacor F, Luzi L, Massa M, Ameri G (2009) The Mw 6 3, 2009 L'Aquila earthquake: source, path and site effects from spectral analysis of strong motion data. Geophys J Int 179:1573–1579

Blumetti AM, Di Filippo M, Zaffiro P, Marsan P, Toro B (2002) Seismic hazard characterization of the city of L'Aquila (Abruzzo, Central Italy): new data from geological, morphotectonic and gravity prospecting analyses. Studi Geologici Camerti: 7-18

Bommer JJ, Acevedo AB (2004) The use of real earthquake accelerograms as input to dynamic analysis. J Earthq Eng 8(spec01):43–91

Boore DM (2003) Simulation of ground motion using the stochastic method. Pure Appl Geophys 160:635–676

Borghini A, Del Monte E, Ortolani B, Vignoli A (2011) Studio degli effetti del sisma del 06/04/2009 sulla Frazione di Castelnuovo, Comune di San Pio delle Camere (AQ). In: Atti del XIV Convegno Nazionale ANIDIS "L'ingegneria sismica in Italia", Bari (in Italian)

Bosi C, Bertini T (1970) Geologia della media valle dell'Aterno. Memorie della Società Geologica Italiana 9:719–777

Chiarabba C, Amato A, Anselmi M, Baccheschi P, Bianchi I, Cattaneo M, Cecere G, Chiaraluce L, Ciaccio MG, De Gori P, De Luca G, Di Bona M, Di Stefano R, Faenza L, Govoni A, Improta L, Lucente FP, Marchetti A, Margheriti L, Mele F, Michelini A, Monachesi G, Moretti M, Pastori M, Piana Agostinetti N, Piccinini D, Roselli P, Seccia D, Valoroso L (2009) The 2009 L'Aquila (central Italy) MW6 3 earthquake: main shock and aftershocks. Geophys Res Lett 36:L18308–L18314

Chiaraluce L, Valoroso L, Piccinini D, Di Stefano R, De Gori P (2011) The anatomy of the 2009 L'Aquila normal fault system (central Italy) imaged by high-resolution foreshock and aftershock locations. J Opehys Res 116:B12311. doi:10.1029/2011JB008352

Chioccarelli E, Iervolino I (2010) Near-source seismic demand and pulse-like records: a discussion for L'Aquila earthquake. Earthq Eng Struct Dynam 39(9):1039–1062

Cirella A, Piatanesi A, Tinti E, Chini M, Cocco M (2012) Complexity of the rupture process during the 2009 L'Aquila, Italy, earthquake. Geophys J Int 190:607–621

Costanzo A (2007) Analisi di fenomeni deformativi di pendii e rilievi in condizioni sismiche: il caso di Gerace. Ph D thesis in Geotechnical Engineering, University of Calabria (in Italian)

Coutant O (1994) Expression of the Green's functions in cylindrical coordinates used with a reflectivity method, Axitra program ftp://lgit.obs.ujfgrenoble.fr/pub/archive/axitra/axitra.ps

Cupillard P, Delavaud E, Burgos G, Festa G, Vilotte JP, Capdeville Y, Montagner JP (2012) RegSEM: a versatile code based on the spectral element method to compute seismic wave propagation at the regional scale. Geophys J Int 188(3):1203–1220

Del Gaudio S, Festa G, Causse M (2015) Strong motion numerical simulations using the empirical Green's function method: application to 2009 L'Aquila earthquake. Geophys J Int 203(1):720–736

Donahue JL, Abrahamson NA (2014) Simulation-based hanging wall effects. Earthq Spectra 30(3):1269–1284

Douglas J, Aochi H (2008) A survey of techniques for predicting earthquake ground motions for engineering purposes. Surv Geophys 29(3):187–220

Evangelista L, Landolfi L, d'Onofrio A, Silvestri F (2016) The influence of the 3D morphology and cavity network on the seismic response of Castelnuovo hill to the 2009 Abruzzo earthquake. Bull Earthq Eng 14(12):3363–3387. doi:10.1007/s10518-016-0011-8

Galadini F, Galli P (2000) Active tectonics in the central Apennines (Italy) e input data for seismic hazard assessment. Nat Haz 22:225–270

Gallipoli MR, Bianca M, Mucciarelli M, Parolai S, Picozzi M (2013) Topographic versus stratigraphic amplification: mismatch between code provisions and observations during the L'Aquila (Italy 2009) sequence. Bull Earthq Eng 11(5):1325–1336. doi:10.1007/s10518-013-9446-3

Gallovic F, Brokesová J (2008) Probabilistic Aftershock Hazard Assessment II: application of Strong Ground Motion Modeling. J Seismol 12(1):65–78

Gallovic F, Zahradník J (2011) Complexity of the M6 3 2009 L'Aquila (central Italy) earthquake: 1 Multiple finite-extent source inversion. J Geophys Res 117:B04307

Gallovič F, Imperatori W, Mai PM (2015) Effects of three-dimensional crustal structure and smoothing constraint on earthquake slip inversions: case study of the Mw6.3 2009 L'Aquila earthquake. J Geophys Res Solid Earth 120:428–449. doi:10.1002/2014JB011650

Ge.Mi.Na. (1963) Ligniti e torbe dell'Italia continentale. "Gemina" Geomineraria Nazionale, Roma

Giaccio B, Galli P, Messina P, Peronace E, Scardia G, Sottili G, Silvestri S (2012) Fault and basin depocentre migration over the last 2 Ma in the L'Aquila 2009 earthquake region, central Italian Apennines. Quatern Sci Rev 56:69–88. doi:10.1016/j.quascirev.2012.08.016

Hartzell SH (1978) Earthquake aftershocks as Green's functions. Geophys Res Lett 5:1–4

Hashash YMA, Park D (2002) Viscous damping formulation and high-frequency components in deep deposits. Soil Dyn Earthq Eng 22(7):611–624

Iervolino I, De Luca F, Cosenza E (2010a) Spectral shape-based assessment of SDOF nonlinear response to real, adjusted and artificial accelerograms. Eng Struct 32(9):2776–2792

Iervolino I, Galasso C, Cosenza E (2010b) REXEL: computer aided record selection for code-based seismic structural analysis. Bull Earthq Eng 8:339–362

Iervolino I, Galasso C, Paolucci R, Pacor F (2011) Engineering ground motion record selection in the ITalian ACcelerometric Archive. Bull Earthq Eng 9(6):1761–1778

Improta L, Villani F, Bruno PP, Castiello A, De Rosa D, Varriale F, Giacomuzzi G (2012) High-resolution controlled-source seismic tomography across the Middle Aterno basin in the epicentral area of the 2009, Mw 6 3, L'Aquila earthquake (central Apennines, Italy). Ital J Geosci 131(3):373–388. doi:10.3301/IJG.2011.35

Irikura K (1983) Semi-empirical estimation of strong ground motions during large earthquakes. Bull. Disast. Prev. Res. Inst Kyoto Univ. 3:63–104

ITASCA 2006 FLAC—Fast Lagrangian Analysis of Continua Version 7 Itasca Consulting Group Inc

Koketsu K, Miyake H (2008) A seismological overview of long-period ground motion. J Seismol 12(2):133–143

Komatitsch D, Liu Q, Tromp J, Süss P, Stidham C, Shaw JH (2004) Simulations of Ground Motion in the Los Angeles Basin Based upon the Spectral-Element Method. Bull Seismol Soc Am 94(1):187–206

Landolfi L, Evangelista L, Chiaradonna A, d'Onofrio A, Silvestri F (2014) Analisi della risposta sismica locale del colle di Castelnuovo. In Atti del XXV Convegno Nazionale AGI: La Geotecnica nella difesa del territorio e delle infrastrutture dalle calamità naturali Baveno 2:177–184 AGI Roma (in Italian)

Lanzo G, Silvestri F, Costanzo A, d'Onofrio A, Martelli L, Pagliaroli A, Sica S, Simonelli A (2011a) Site response studies and seismic microzoning in the middle Aterno Valley (L'Aquila, Central Italy). Bull Earthq Eng 9(5):1417–1442. doi:10.1007/s10518-011-9278-y

Lanzo G, Tallini M, Milana G, Di Capua G, Del Monaco F, Pagliaroli A, Peppoloni S (2011b) The Aterno valley strong-motion array: seismic characterization and determination of subsoil model. Bull Earthq Eng 9(6):1855–1875

Locati M, Camassi R, Stucchi M. (2011) DBMI11, la versione 2011 del Database Macrosismico Italiano 2011. Milano, Bologna. http://emidius.mi.ingv.it/DBMI11. doi:10.6092/INGV.IT-DBMI11

Lucca E, Festa G, Emolo A (2012) Kinematic inversion of strong motion data using a Gaussian parameterization for the slip: application to the 2008 Iwate-Miyagi, Japan, earthquake. Bull Seismol Soc Am 102(6):2685–2703

Lysmer J, Kuhlemeyer RL (1969) Finite Dynamic Model for Infinite Media. J Soil Mech Found Div ASCE 95(SM4):859–877

Magnoni F, Casarotti E, Michelini A, Piersanti A, Komatitsch D, Tromp J (2014) Spectral-Element Simulations of Seismic Waves generated by the 2009 L'Aquila earthquake. Bull Seismol Soc Am 104(1):73–94. doi:10.1785/0120130106

Mai PM, Beroza GC (2002) A spatial random-field model to characterize complexity in earthquake slip. J Geophys Res 107(B11):2308. doi:10.1029/2001JB000588

Mancini M, Cavuoto G, Pandolfi L, Petronio C, Salari L, Sardella R (2012) Coupling basin infill history and mammal biochronology in a Pleistocene intramontane basin: the case of western L'Aquila Basin (central Apennines, Italy). Quatern Int 267:62–77. doi:10.1016/j.quaint.2011.03.020

Mazzieri I, Stupazzini M, Guidotti R, Smerzini C (2013) SPEED: SPectral Elements in Elastodynamics with Discontinuous Galerkin: a non-conforming approach for 3D multi-scale problems. Int J Numer Meth Eng 95(12):991–1010

Monaco P, Totani G, Barla G, Cavallaro A, Costanzo A, d'Onofrio A, Evangelista L, Foti S, Grasso S, Lanzo G, Madiai C, Maraschini M, Marchetti S, Maugeri M, Pagliaroli A, Pallara O, Penna A, Saccenti A, Santucci de Magistris F, Scasserra G, Silvestri F, Simonelli AL, Simoni G, Tommasi P, Vannucchi G, Verrucci L (2012) Geotechnical aspects of the L'Aquila earthquake. In: Sakr M A, Ansal A(eds) Special Topics in Earthquake Engineering, Geotechnical, Geological and Earthquake Engineering 16, Springer chapter 1: 1–66, ISBN: 9789400720596. doi:10.1007/978-94-007-2060-2_1

Motazedian D, Atkinson G (2005) Stochastic finite-fault model based on dynamic corner frequency. Bull Seismol Soc Am 95:995–1010

NIST (2011) Selecting and scaling earthquake ground motions for performing response-history analyses. NIST GCR 11-917-15, Prepared by the NEHRP Consultants Joint Venture for the National Institute of Standards and Technology, Gaithersburg

Olsen KB, Day SM, Minster JB, Cui Y, Chourasia A, Faerman M, Moore R, Maechling P, Jordan T (2006) Strong shaking in Los Angeles expected from southern San Andreas earthquake. Geophys Res Lett 33:L07305. doi:10.1029/2005GL025472

Ortolani B, Borghini A, Boschi S, Del Monte E, Vignoli A (2012) Study of vulnerability and damage: thecase study of Castelnuovo after L'Aquila earthquake (Italy). In: Proceedings of 15 World Conference Earthquake Engineering, Lisbon, Paper ID 4439

Paolucci R, Mazzieri I, Smerzini C, Stupazzini M (2014) Physics-Based Earthquake Ground Shaking Scenarios in Large Urban Areas. In: Perspectives on European Earthquake Engineering and Seismology. Springer, Berlin, pp 331–359

Paolucci R, Mazzieri I, Smerzini C (2015) Anatomy of strong ground motion: near-source records and 3D physics-based numerical simulations of the Mw 6.0 May 29 2012 Po Plain earthquake. Italy. Geophys J Int 203:2001–2020

Poiata N, Koketsu K, Vuan A, Miyake H (2012) Low-frequency and broad-band source models for the 2009 L'Aquila, Italy, earthquake. Geophys J Int 191(1):224–242. doi:10.1111/j.1365-246X.2012.05602.x

Porter K, Jones L, Cox D, Goltz J, Hudnut K, Mileti D, Perry S, Ponti D, Reichle M, Rose AZ, Scawthorn CR, Seligson HA, Shoaf KI, Treiman J, Wein A (2011) The ShakeOut Scenario: a hypothetical Mw7. 8 earthquake on the southern San Andreas fault. Earthq Spectra 27:239–261

Sabetta F, Pugliese A (1996) Estimation of response spectra and simulation of nonstationary earthquake ground motions. Bull Seism Soc Am 86:337–352

Santo A, Ascione A, Di Crescenzo G, Miccadei E, Piacentini T, Valente E (2014) Tectonic-geomorphological map of the middle Aterno River valley (Abruzzo, Central Italy). J Maps 10(3):365–378. doi:10.1080/17445647.2013.867545

Santucci de Magistris F, d'Onofrio A, Evangelista L, Foti S, Maraschini M, Monaco P, Amoroso S, Totani G, Lanzo G, Pagliaroli A, Madiai C, Simoni G, Silvestri F (2013) Geotechnical characterization of the Aterno Valley for site response analysis. Riv Ital di Geotec 43(3):23–43

Scognamiglio L, Tinti E, Michelini A, Dreger D, Cirella A, Cocco M, Mazza S, Piatanesi A (2010) Fast determination of moment tensors and rupture history: application to the April 6th 2009. L'Aquila Earthq Seismol Res Lett 81(6):892

Sica S, Dello Russo A, Rotili F, Simonelli AL (2013) Ground motion amplification due to shallow cavities in nonlinear soils. Nat Hazards. doi:10.1007/s11069-013-0989-z

Smerzini C, Villani M (2012) Broadband numerical simulations in complex near field geological configurations: the case of the MW 6 3 2009 L'Aquila earthquake. Bull Seismol Soc Am 102:2436–2451

Smerzini C, Galasso C, Iervolino I, Paolucci R (2014) Ground motion record selection based on broadband spectral compatibility. Earthq Spectra 30(4):1427–1448

Tallini M, Cavuoto G, Del Monaco F, Di Fiore V, Mancini M, Caielli G, Rapolla A (2012) Seismic surveys integrated with geological data for in-depth investigation of Mt Pettino active fault area (western L'Aquila basin). Ital J Geosci 131(3):389–402. doi:10.3301/IJG.2012.10

Tinti E, Scognamiglio L, Cirella A, Cocco M (2014) Up-dip directivity in near-source during the 2009 L'Aquila mainshock. Geophys J Int 198:1618–1631

Working Group MS-AQ (2010) Microzonazione sismica per la ricostruzione dell'area aquilana. Dipartimento della Protezione Civile—Regione Abruzzo (in Italian)